Ecology, 73(2), 1992, pp. 479–494

ON THE SPATIAL SPREAD OF INSECT PATHOGENS: THEORY AND EXPERIMENT[1]

GREG DWYER[2]
Department of Zoology, University of Washington, Seattle, Washington 98195 USA

Abstract. The mathematical theory of animal diseases has seen explosive growth in the past decade, yet most of the existing theory examines only temporal disease spread, ignoring the effects of patchy host or pathogen spatial distributions. Here I present a model for the within-season spatial spread of insect pathogens that incorporates host movement in an otherwise conventional insect host–pathogen model. Mathematical analysis of the model reveals that the pathogen will spread through the host population in a moving wave front of disease, known as a "travelling wave." This analysis shows how the spatial rate of spread of the pathogen depends upon the transmission rate of the disease, the rate of production of the pathogen by infected hosts, the initial population of the host, the decay rate of the pathogen, and the death rate of infected hosts.

To test the predictions of the model, I performed a series of field experiments with the nuclear polyhedrosis virus (NPV) of Douglas-fir tussock moth, *Orgyia pseudotsugata*. First, I estimated each of the parameters of the model in the field with a series of small-scale experiments, and used the parameter estimates to predict the spatial rate of spread of the NPV through a population of tussock moth larvae (NPV diseases, like many insect pathogens, do not infect adults). To test this prediction, I then performed an experiment in which I measured the rate of spread of the NPV in an experimental population of tussock moth larvae on linear arrays of Douglas-fir seedlings. The model predicts the rate of spread of tussock moth NPV fairly accurately, suggesting that one can use this type of model to extrapolate individual behavior and localized transmission patterns to broader-scale spatial dynamics.

Key words: biological control; disease transmission; Douglas-fir tussock moth; epizootiology; host–parasite; mathematical epidemiology; model of spatial spread of disease; nuclear polyhedrosis virus; population biology of disease; reaction–diffusion; spatial spread; travelling wave.

INTRODUCTION

Models describing the dynamics of infectious diseases in animal populations represent one of the best-developed areas of mathematical ecology (Anderson et al. 1981, Anderson and May 1981, Levin and Pimentel 1981, Hochberg 1989, Dwyer et al. 1990). Nevertheless, like most ecological theory, models of animal diseases largely have been based on the assumption that spatial structure is of negligible importance; that is, most models assume that the spatial distributions of host and pathogen are unimportant. Many of the existing models that do include spatial structure require a knowledge of how transmission varies with distance from the pathogen (so-called "contact distribution models" [Mollison 1977, Thieme 1977, Diekmann 1979]). Since transmission by this definition would be hard to measure for mobile hosts, applications of this theory have been restricted to plant diseases (van den Bosch et al. 1988*a, b, c*). In this paper I analyze and test a model of insect pathogens in which spatial structure plays a central role. My goal is to develop a model that is simple enough to provide a general theoretical framework for the spatial dynamics of insect pathogens, yet is realistic enough to allow predictions of their rate of spatial spread. The model that I use (a so-called "reaction–diffusion model" [Kendall 1965, Murray et al. 1986, Murray 1989]) requires only a local measurement of transmission, and thus can be applied easily to real insect host–pathogen systems.

Although spatial structure has been shown to be important in a number of insect host–pathogen systems (see Entwistle et al. [1983] for a review), the lack of an appropriate spatially structured theory has made it difficult to understand the existing field data. Part of my intent in this paper is to provide a basic theoretical background to aid in identifying the mechanisms driving the spatial spread of insect pathogens. More generally, since pathogens play an important role in the dynamics of an enormous number of insects (Kaya and Anderson 1976, Harkrider and Hall 1978, Myers 1981, Fuxa 1982, Kalmakoff and Crawford 1982, Carter et al. 1983, Entwistle et al. 1983, Murdoch et al. 1985, Fleming et al. 1986), and are widely used as biological insecticides (Thompson and Steinhaus 1950, Bird and Burk 1961, Stairs 1965, Klein and Podoler 1978,

[1] Manuscript received 9 November 1990; revised 22 April 1991; accepted 8 May 1991; final version received 5 June 1991.

[2] Present address: Department of Entomology, Fernald Hall, University of Massachusetts, Amherst, Massachusetts 01003 USA.

McLeod et al. 1982, Mohamed et al. 1983, Podgwaite et al. 1984, Shepherd et al. 1984, Fuxa 1987, Otvos et al. 1987), an understanding of their spatial dynamics will contribute to both basic insect ecology and insect pest management.

For the purpose of testing the model I focus on a particular insect–pathogen system: Douglas-fir tussock moth, *Orgyia pseudotsugata,* and its nuclear polyhedrosis virus or NPV. Douglas-fir tussock moth ranges from southern British Columbia to Arizona and California, and feeds on economically important conifers throughout its range (Brookes et al. 1978). Larvae go through five instars in the male, and six in the female. Females are flightless, and most long-distance dispersal is accomplished by ballooning in the first and sometimes the second instar (Mitchell 1979). Periodically, the tussock moth undergoes outbreaks in which its density increases by >4 orders of magnitude (Brookes et al. 1978); these outbreaks are often terminated by epizootics of the NPV disease. The DNA of NPVs is enclosed in a polyhedral-shaped protein matrix, called a polyhedral inclusion body, which enables the virus to survive outside of the host for long periods and acts as the infectious stage in the viral life cycle. Larvae become infected by accidentally consuming these particles on contaminated foliage; if a larva consumes enough particles at once, it becomes infected, and dies within ≈2 wk. Shortly after the larva dies its integument breaks open, releasing particles into the environment where they can infect new larvae. Because of this mechanism of transmission, only dead larvae are infectious.

In earlier work on this system (Dwyer 1991) I demonstrated that the transmission rate of the disease is partly dependent upon the spatial patchiness of the pathogen, an effect that appears to be modulated by the movement rate of the host. By building on these empirical results, the present paper is an attempt to explore mathematically the consequences of pathogen patchiness and host movement for the spatial spread of the pathogen. Although I focus here on pathogen spread from a point source through a uniformly distributed host population, the model can be used to represent the disease dynamics resulting from any initial distribution of host and pathogen.

Because this paper contains both the development of a general model, and an experimental test of the model with a specific system, its organization is not standard. In the first two sections I describe the model and analyze the range of behaviors that it can exhibit. In the third section, I describe a set of experiments that were used to estimate parameters in the model, and an experiment designed to test the model, in which I compared the model's predictions to the outcome of experimentally initiated epizootics. Finally, in the *Discussion,* I consider the generality of the model, and its successes and failures in the specific case of the NPV of Douglas-fir tussock moth.

The Model

As Anderson and May (1981) observe, what makes many insect pathogens different from other animal diseases is the presence of long-lived infectious stages that are capable of surviving for extended periods outside of the host. Such so-called "free-living" stages are not confined to viruses; fungal pathogens and microsporidia, for example, also have long-lived infectious stages (Carruthers and Soper 1987, Maddox 1987). Since my immediate concern is with viruses, I will here deemphasize fungi and microsporidia. However, the model that I present is not specific to a particular pathogen taxon. The standard approach to modelling insect diseases involving free-living pathogens is to construct three differential equations, one each for the density of susceptible hosts (S), the density of infectious hosts (I) and the density of free-living pathogen particles (P) (Anderson and May 1981):

$$\frac{dS}{dT} = r(S + I) - \nu PS; \tag{1}$$

$$\frac{dI}{dT} = \nu PS - \alpha I; \quad \text{and} \tag{2}$$

$$\frac{dP}{dT} = \lambda I - [\mu + (S + I)]P, \tag{3}$$

where r is the reproductive rate of the host, ν is the transmission coefficient, α is the rate of disease induced mortality, λ is the rate of production of pathogen particles by infected hosts, μ is the decay rate of the pathogen, and T is time. This system of equations describes how epizootics develop in systems in which host and pathogen are said to be "well-mixed." In other words, either (1) the host or the pathogen (or both) is very mobile or (2) the host and pathogen spatial distributions are uniform; in either case, spatial distribution may be unimportant. Not surprisingly, these conditions are often violated for *actual* insect host–pathogen systems (Entwistle et al. 1983).

In the present paper I consider only host–pathogen dynamics within a season. This is because a single season represents an experimentally tractable time scale and because in practical applications, such as the use of pathogens as biological insecticides, we are concerned primarily with within-season spread (Shepherd et al. 1984, Otvos et al. 1987). Restricting the model to within-season dynamics allows me to simplify Eqs. 1–3 in two ways. First, there is no reproduction of the host within a season. Second, the amount of virus consumed by the host within a season (virus consumption is represented by the $\nu(S + I)P$ term in Eq. 3) is probably negligible compared to the amount produced by infected hosts, as λ and μ are typically much larger than ν (Anderson and May 1981; also see *Predicting the spatial spread of the NPV of Douglas-fir tussock moth,* below. Relaxing this assumption has no effect on the

calculated rate of spread of the pathogen). The simplified model is thus:

$$\frac{dS}{dT} = -\nu PS; \tag{4}$$

$$\frac{dI}{dT} = \nu PS - \alpha I; \quad \text{and} \tag{5}$$

$$\frac{dP}{dT} = \lambda I - \mu P. \tag{6}$$

I have examined the ability of this model to describe the local transmission dynamics of the NPV of tussock moth, and have found that it works well if all hosts are in the same developmental stage (Dwyer 1991). Here I extend the model to include spatial dynamics by allowing for the movement of host and pathogen. This is done by adding a term to Eqs. 4 and 5 that represents larval movement (typically only larvae can become infected); since the model now keeps track of changes in both space and time, the ordinary differential equations become partial differential equations. Movement is represented as diffusion, which is equivalent to assuming that larvae move randomly in all possible directions (Okubo 1980). This approximation is appropriate for many insects (Kareiva 1983), including Douglas-fir tussock moth larvae, as I show in *Predicting the spatial spread . . . : Parameter estimation,* below. Incorporating more complex host movement into the model would be straightforward (Okubo 1980), although it might complicate the analysis.

The resulting spatially structured model is:

$$\frac{\partial S(X,T)}{\partial T} = -\nu PS + D\frac{\partial^2 S}{\partial X^2}; \tag{7}$$

$$\frac{\partial I(X,T)}{\partial T} = \nu PS - \alpha I + D\frac{\partial^2 I}{\partial X^2}; \quad \text{and} \tag{8}$$

$$\frac{\partial P(X,T)}{\partial T} = \lambda I - \mu P. \tag{9}$$

The symbols here are the same as in Eqs. 4–6, with the exception that the susceptible population S, the infected population I, and the pathogen population P are now functions of both time T and distance X. In addition, the $D\frac{\partial^2}{\partial X^2}$ terms represent host movement, where the diffusion coefficient D is a measure of dispersal rate.

In the present paper the model is confined to one spatial dimension. Although the spatial spread of insect diseases in the field of course occurs in two dimensions, the one-dimensional model simplifies both the analysis and the experimental test. Moreover, the dynamics of one-dimensional disease models with dispersal are often qualitatively similar to the dynamics of their two-dimensional counterparts (Murray et al. 1986). Finally, in many situations one dimension may well be a reasonable approximation. For example, when a pathogen spreads outward from a point, the disease front that develops may be nearly circular. At long enough time intervals, a spreading circle will present an essentially planar front in each direction, since a circle with a large enough radius viewed at a local scale looks like a straight line. In such cases, the spread in any particular direction can be approximated with one dimension. Because of this, when insect viruses are used in biological control their spread is often described in terms of one dimension (Entwistle et al. 1983, Otvos et al. 1987).

Analysis of the Model

One of the important features of the class of model represented by Eqs. 7–9 is that such models can exhibit what is known as "travelling wave behavior" (Murray 1989). For the present model, this means that the spatial distribution of the infected fraction of the population develops into a moving wave front of disease. As it moves across the landscape, this front is simply a transition zone between high disease incidence close to the source of the disease and low disease incidence far from the source of the disease (Fig. 1). Significantly, the front will maintain its shape if the spatial scale is large enough that boundary effects are not important.

Although travelling waves may seem abstract, existing data on the spatial spread of insect viruses in the field suggest that such waves exist in nature. In each of the field studies reviewed by Entwistle et al. (1983), the spatial distribution of the infected fraction of the population looks and moves very much like a travelling wave. Computer simulations of the model Eqs. 7–9 demonstrated that travelling waves with constant shape occur in the model as well. This indicates that a more formal analytical exploration of travelling wave behavior may be possible (described in detail in Appendix A). Travelling wave analysis has received scant attention from field ecologists (but see van den Bosch et al. 1990, Manasse and Kareiva 1991), which is unfortunate because it is a major tool for exploring spatially distributed population phenomena, and often can be understood with little more than linear stability analysis of ordinary differential equations (Odell 1981). Briefly, the analysis consists of transforming the model to a moving coordinate system. This reduces the partial differential equations—Eqs. 7–9, which are functions of space X and time T—to ordinary differential equations, which are functions of a new "dummy" variable ξ and a new *parameter* c (according to the transformation $\xi = X + cT$). The new parameter c is the rate of advance of the wave of disease, or the wave speed. This transformation allows me to analyze the model as a system of ordinary differential equations.

As in linear stability analysis, the analysis begins with the identification of the equilibrium points. For Eqs. 4–6 there are two equilibrium points

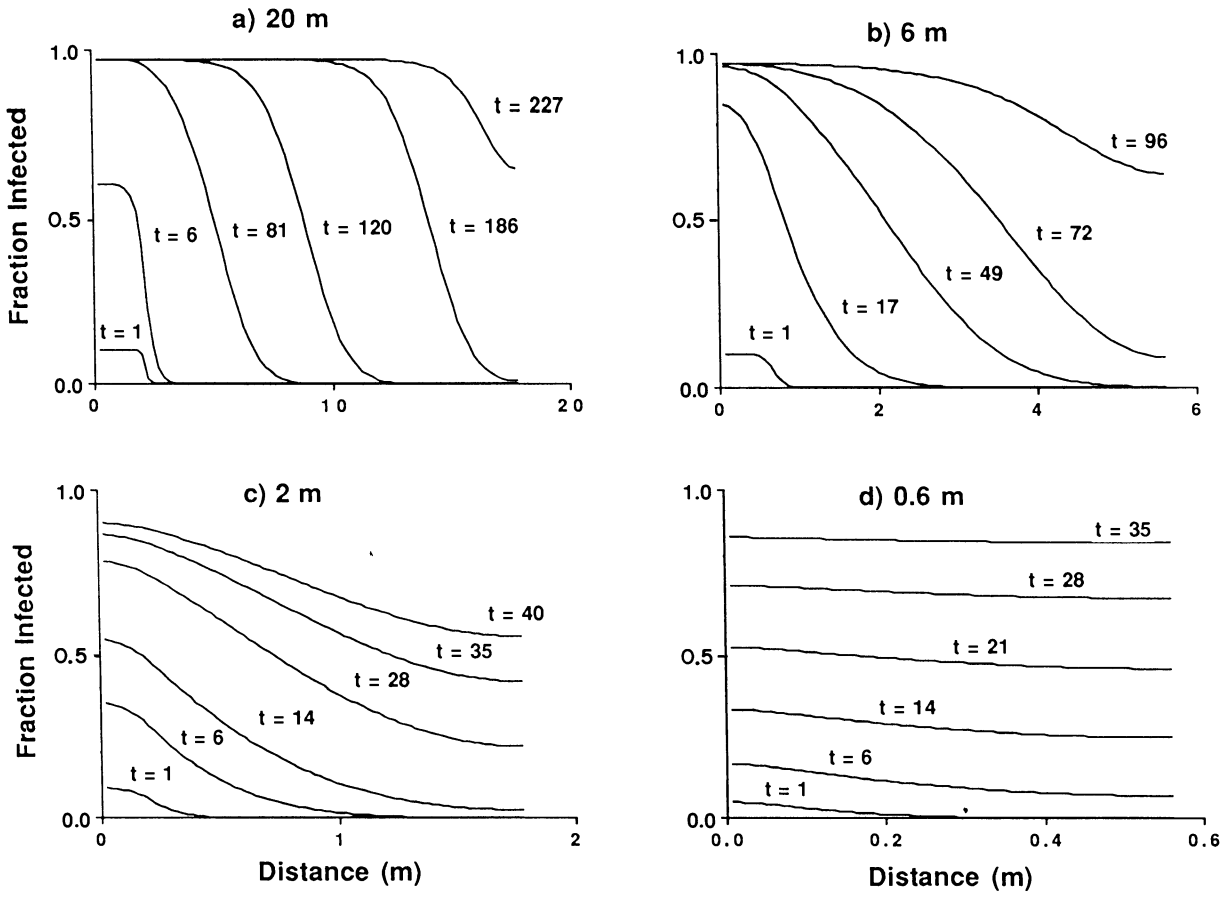

FIG. 1. Travelling wave fronts of disease in an insect population. All the curves were generated by numerical simulation of Eqs. 4–6. For each graph the time (t) between successive curves is indicated in days. The parameters for all four graphs are the same (Table 1); the only difference is the location of a barrier beyond which the insect hosts cannot move. The distance between the source of the disease and the barrier is indicated at the top of each graph: (a) 20 m, (b) 6 m, (c) 2 m, and (d) 0.6 m. Note that as the spatial scale is reduced, in other words as the barrier moves closer to the source of the disease, the waves maintain their shape for shorter time intervals. The constancy of shape over time varies from (a), in which there is a long series of unchanging waves, to (d), in which the front of disease is very close to uniform almost immediately. Also, in all cases, there is an effect of the initially small quantity of pathogen particles. In (a), for example, it takes almost 80 d before an unchanging wave develops. (c) represents the scale of the experimental test of the model (see *Predicting the spatial spread of the NPV of Douglas-fir tussock moth*).

$$(S,I,P) = (0,0,0) \quad \text{and} \tag{10}$$

$$(S,I,P) = (S_0,0,0), \tag{11}$$

where S_0 is the initial population of susceptibles. I assume that the initial susceptible population is uniformly distributed (so that $S[X,0]$ can be written $S[0]$); the analysis requires this assumption, although the simulations do not. With this initial condition, a travelling-wave solution to the model consists of a wave of disease that transforms one spatially uniform equilibrium into another. The simulations indicate that, as in the model without spatial structure (i.e., Eqs. 4–6), there is a threshold value of the susceptible population. For the non-spatial model, this threshold is the minimum value necessary for an epizootic to occur. For the spatial model the threshold for an epizootic is also the threshold for a travelling wave. That is, for

$$S_0 < \frac{\mu\alpha}{\nu\lambda} \tag{12}$$

no wave forms; instead, the disease barely spreads from the point of its introduction. For

$$S_0 > \frac{\mu\alpha}{\nu\lambda} \tag{13}$$

a travelling wave occurs. In front of the wave, the population of susceptibles is equal to S_0, and the population of the infected hosts and pathogen particles is equal to 0. Behind the wave the population of susceptibles trails away to a new spatially uniform equilibrium, and the populations of infected hosts and pathogen particles trail away to 0 asymptotically.

In Appendix A I derive an expression for the minimum possible wave speed. Although it is extremely

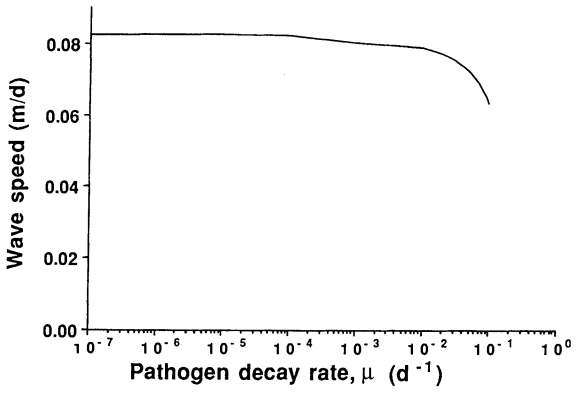

FIG. 2. Rate of advance or wave speed c of the tussock moth nuclear polyhedrosis virus vs. the pathogen decay rate μ. The values of the other parameters are the same as in Table 1.

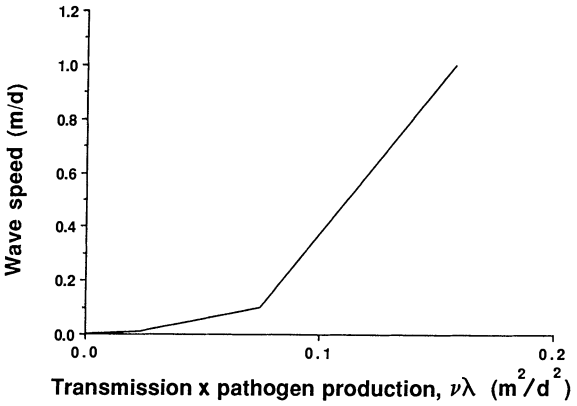

FIG. 4. Wave speed c of the spread of tussock moth nuclear polyhedrosis virus vs. the parameter combination $\nu\lambda$. The other parameters are the same as in Table 1.

difficult to prove that waves travelling at this speed are the stable ones, I found that waves in numerical simulations travel at the calculated minimum speed for a wide range of parameter values. This suggests that the analytically calculated minimum wave speed is indeed the speed of the wave. Similar results have been found for other disease models (Thieme 1977, Diekmann 1979, Murray et al. 1986). The usefulness of calculating the wave speed is that it provides a single parameter giving the rate of spread of the disease. Often this is what we are most interested in, rather than the particular shape of the wave. Moreover, the wave speed summarizes the relationship between the rate of spread of the disease and the model parameters. It combines the individual-level processes of disease transmission, disease induced mortality, production of virus particles, virus decay, and host movement into a single measure for the population-level phenomenon of disease spread. This emphasizes that the model makes predictions at the level of the population, using parameters that are for the most part estimated at the level of the individual (Hassell and May 1985).

An important caveat is that the initial velocity of the wave of disease will depend upon the initial conditions. For example, if the disease is introduced in the form of only a few pathogen particles, it can take a substantial period of time for a wave front of disease to reach the calculated velocity (Fig. 1). Similarly, as the wave front approaches the edge or boundary of a habitat, it will begin to change shape. As the spatial scale of the habitat becomes smaller, these two effects will combine to distort the wave front over the entire area of the epizootic (Fig. 1). In summary, the calculated wave speed describes the long-term rate of spread of the pathogen in a large-scale habitat, while the simulations can describe both initial disease spread and spread at small habitat scales.

Figs. 2, 3, 4, and 5 depict the dependence of the wave speed on the model parameters, summarizing the model behavior with respect to each parameter. The direc-

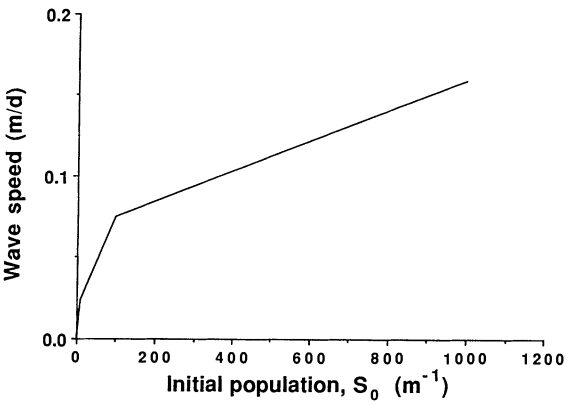

FIG. 3. Wave speed c of the spread of tussock moth nuclear polyhedrosis virus vs. size of the initial susceptible host population, S_0. The other parameters are the same as in Table 1.

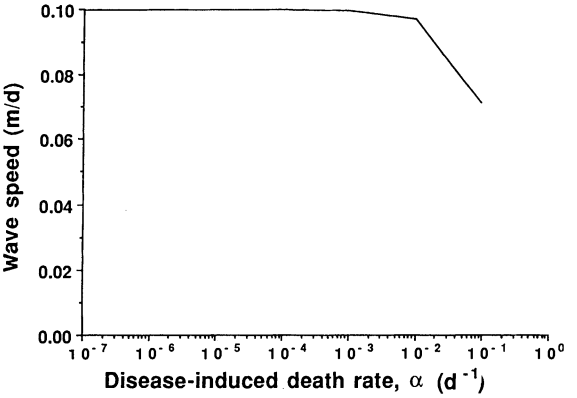

FIG. 5. Wave speed c of the spread of tussock moth nuclear polyhedrosis virus vs. the disease-induced larval mortality rate α. The other parameters are the same as in Table 1.

tion of this dependence is in accord with intuition; that is, the rate of spatial spread of the disease increases with increasing pathogen longevity (Fig. 2: decreasing μ), increasing initial host population (Fig. 3: S_0), increasing transmission rate or pathogen production rate (Fig. 4: $\nu\lambda$), increasing diffusion rate (linearly with $\sqrt{D}$: see Appendix A), and increasing longevity of infected larvae (Fig. 5: lower α).

Figs. 2–5 also indicate the sensitivity of the model to each parameter, which provides guidance on how accurately each of these parameters must be estimated. For instance, a 10-fold increase in the decay rate of the pathogen μ produces at most a 30% decrease in the wave speed, indicating that I do not need a very exact estimate of the decay rate in order to predict the wave speed. This information also could be used to understand how different strains of a pathogen will vary in the rate at which they spread spatially, which would be useful in evaluating the efficacy of different strains for pest control.

Predicting the Spatial Spread of the NPV of Douglas-Fir Tussock Moth

Testing whether the model Eqs. 7–9 can be used to extrapolate from the behavior of individual Douglas-fir tussock moth (DFTM) larvae to patterns of disease spread poses two separate experimental problems. The first is estimating the parameters of the model, and the second is testing the model prediction that arises from the parameter estimates. In the summer of 1989 I performed a series of experiments in which I first independently estimated the parameters of the model, and second tested the prediction of the model. Estimating the parameters is fairly easy, as most of them can be estimated at a small scale. Testing the model prediction experimentally is logistically difficult, because the model requires the introduction of the disease into a disease-free population that is dense enough to permit disease spread. Also, as the population declines as a result of the disease, stochastic effects will become more important, yet the model is deterministic. Although the experimental test that I present suffers from these difficulties, it nevertheless usefully illustrates the procedure of testing the model.

Parameter estimation

I separated the problem of parameter estimation into four steps: (1) estimating the decay rate of the virus, μ; (2) estimating the disease-induced mortality rate, α; (3) estimating the transmission rate, ν, times the pathogen production rate, λ; (4) estimating the diffusion coefficient, D. The first three of these represent the interaction between host and pathogen; it turned out to be possible to estimate all of these parameters from the same experiment. I then used an additional experiment to estimate the diffusion coefficient.

All the experiments were carried out in an area of second-growth Douglas-fir/grand fir (*Pseudotsuga menziesii/Abies grandis*) forest in northern Idaho that has a history of tussock moth outbreaks and virus epizootics. Because transmission rates vary with larval instar (Dwyer 1991), for both the experimental estimates of the parameters and the experimental test of the model I used only fifth-instar larvae.

Disease parameters (μ, ν, λ, α).—To estimate the parameters describing the dynamics of the host–pathogen interaction, I reared healthy larvae on a pair of seedling Douglas-fir containing infected cadavers, and counted the number of larvae that became infected as a result of contact with the cadavers (only larvae can become infected, since adults do not feed). The Douglas-fir were planted in wading pools, with a sticky substance (Tanglefoot) around the top of the wading pool that the larvae will not touch: this prevents larvae from leaving the experimental arena (Dwyer 1991). Around each wading pool I placed a 1.2-m^3 cage made of spunbonded polyester (Reemay), which prevents predation by vespid wasps yet admits >95% of ambient sunlight.

Both initially healthy larvae and initially infected larvae (which I will refer to as "primary infecteds") were reared in the laboratory from eggs of the GL-1 strain of Douglas-fir tussock moth (Martignoni and Iwai 1980; eggs provided by Paul Iwai). To ensure that larvae were not accidentally contaminated with the virus, all eggs were surface-sterilized in a 10% bleach solution (Robertson 1985). Primary infecteds were infected by being fed artificial diet contaminated with a dose high enough to ensure 100% mortality (1 mL of a solution of 40 infected third-instar cadavers ground up in 100 mL of distilled water).

The healthy and primary-infected larvae were added to the trees ≈24 h before the primary-infected larvae died. Before the primary infecteds were added to the trees they were marked with fluorescent powder to distinguish them from subsequent infections. I censused each pair of trees every other day, at which time I removed for autopsy all dead larvae that were not marked with fluorescent powder. Smears from dead larvae were examined under a light microscope at 400× magnification; presence of polyhedral inclusion bodies, which can be seen easily at this magnification, indicates that a larva died of the virus.

Since all secondary infections were removed shortly after they died, transmission occurred only between the initially healthy larvae and the primary-infected larvae. As will become clear from the methods that I use to estimate each parameter, the rate at which healthy larvae became sick in an experiment can be used to estimate each of the parameters except the diffusion coefficient D.

Estimating the decay rate of the virus: μ.—To measure the rate of virus decay I exposed healthy larvae to infected cadavers of varying ages, which thereby had experienced varying periods of virus decay. In particular, healthy larvae were placed on each pair of trees on 10 August 1989. These trees had received cadavers

either 1, 4, 13, or 32 d prior to 10 August. These four different lead times for the placement of infected cadavers represented the four treatments, which were each replicated twice. One replicate consisted of two seedling Douglas-fir planted in a wading pool, with 50 healthy larvae and 6 infected cadavers placed together on the trees (these densities are within the range of densities observed during natural tussock moth outbreaks [Mason and Thompson 1971, Mason 1981]). In addition, to test for the presence of extraneous virus in the environment or accidental infections in the healthy larvae, I established two controls to which no infected cadavers were added. No infections appeared in either control. The fraction of infected larvae thus serves as a measure of transmission, and the decline in transmission with the age of cadavers can be used to estimate the decay rate of the virus.

Surprisingly, the fraction of larvae that became infected in the virus decay experiment showed no decline with cadaver age (Fig. 6); in other words, over a time period of 32 d virus decay was unmeasureably low. This was probably due to the fact that the experiments were carried out below the forest canopy, where the amount of sunlight is relatively low (Podgwaite et al. 1979, Olofsson 1988). Since virus decay over the period of the experiment was negligible, in the model I assume that the virus half-life is 1 yr; in this range of μ, the wave speed c changes very slightly with decay rate (Fig. 2), so that the particular value of μ is of little consequence. With a half-life of 1 yr, $\mu \approx 0.002$ d^{-1}, which leads to only a 5% loss of virus over 32 d, which is a small enough loss to produce the negligible decay that I observed experimentally.

Disease-induced mortality rate: α.—In the model the disease-induced mortality rate α is assumed to be equivalent to the inverse of the incubation time. Since the incubation time is sensitive to ambient temperature, which fluctuates widely in the field, lab estimates based on constant temperature are not very meaningful. To ensure that my estimate of incubation time would encompass natural temperature variation, I used the time (15 d) until the first infection appeared in either of the two replicates of the 1-d-old cadaver treatment as an estimate of the incubation time, so that α is 1/15 per day. Since Fig. 5 confirms that, in this range of incubation times, the wave speed is relatively insensitive to α, my crude estimation procedure was probably adequate.

Transmission rate ν *and pathogen production rate* λ.—In Appendix A I show that the model can be nondimensionalized so that the transmission coefficient ν and the pathogen production rate λ only appear together as $\nu\lambda$; this means that the model is only affected by these two parameters in combination. Because virus decay was negligible over the space of a month, the 1-d treatment of the decay experiment can be used to estimate $\nu\lambda$ by numerically solving the following equation for $\nu\lambda$ (see Appendix B).

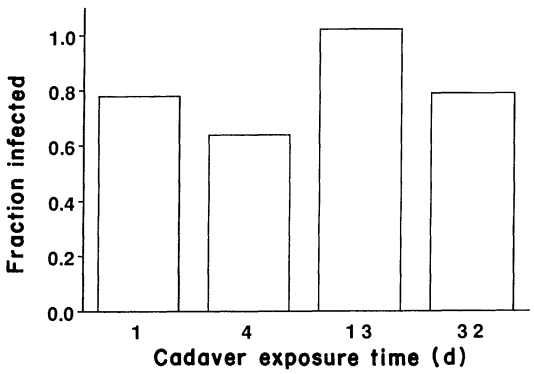

FIG. 6. The effect of different periods of exposure to the environment of NPV-infected tussock moth cadavers on cadaver infectiousness (the virus decay experiment).

$$R(t) = \frac{\nu\lambda I_0 S_0}{\frac{\nu\lambda I_0}{\alpha} - \alpha}\left[\frac{1}{\alpha}(1 - e^{-\alpha t}) - \frac{\alpha}{\nu\lambda I_0}\left(1 - e^{\frac{-\nu\lambda I_0}{\alpha}t}\right)\right], \quad (14)$$

where $R(t)$ is the cumulative number of infections at time t, I_0 is the number of primary infected larvae, and S_0 is the number of initially healthy larvae, and the other parameters are the same as in Eqs. 4–6. Since $R(t)$ represents the observed data, and S_0 and I_0 are known initial conditions of the experiments, $\nu\lambda$ is left as the only unknown in Eq. 14 once a value of the disease-induced mortality rate α has been obtained.

For each of these two replicates $\nu\lambda$ then can be estimated by minimizing the sum of the squared differences (least-squares: Seber [1977]) between the model prediction (Eq. 14) and the time series of the cumulative number of infections. Fig. 7 shows the fit between the model and the time series for each replicate. Considering that there is only one parameter to adjust, the model fits the data fairly well. The resulting value of $\nu\lambda$, averaged over the two replicates, is given in Table 1.

Estimating the host diffusion rate D.—A point release of an insect can be used both to test the assumption of diffusion as a model for movement and to estimate the diffusion coefficient D (Okubo 1980, Kareiva 1983). The diffusion model predicts that, if a group of insects is released at a point in space, then their distribution at any subsequent point in time will approximate a normal curve. Mathematically, the spatial distribution of the dispersing larvae will be

$$p(x,t) = \frac{1}{\sqrt{4\pi Dt}} e^{-x^2/4Dt}. \quad (15)$$

That is, the fraction of larvae at each point in space x at time t, $p(x,t)$, is normally distributed about the release point with mean zero and variance $2Dt$. As a result, the mean squared deviation of the distribution

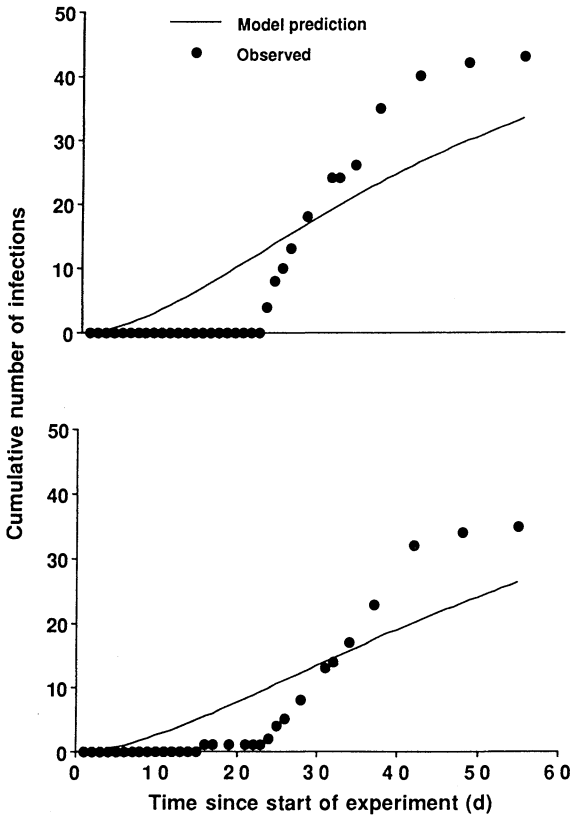

FIG. 7. Time series of virus infections ● in the first two replicates of the virus decay experiment together with the best-fit version —— of Eq. 14.

of insects in space, which is the variance of the normal curve at any one time, will increase linearly through time with slope equal to $2D$. That is,

$$m_t = 2Dt, \qquad (16)$$

where m_t is the mean squared deviation at time t.

On 11 August 1989 I released 40 fifth-instar tussock moth larvae on the third tree of a row of eight seedling Douglas-fir. To ensure that none of the larvae escaped, and to prevent ant predation, the trees were planted in sterile soil on a plastic sheet. Around the edge of the sheet I secured plastic lawn edging that had a coating of Tanglefoot along its top edge. The trees were planted ≈25 cm apart, and the entire setup was ≈2 m in length. I censused the experiment each day for the next 4 d. For this experiment the regression of m_t against time t has a slope of 0.0548 (Fig. 8; $r^2 = 0.995$), so that the diffusion coefficient is 0.0274 m²/d. I used this diffusion coefficient D in Eq. 15 to predict the distribution of larvae at each sampling date (Fig. 9). This is a way of testing the assumption of diffusion; if the larvae are diffusing at a constant rate, then the diffusion coefficient calculated from the regression on *all four* observation dates should be sufficient to describe the shape of the curve on *each* observation date. A Kolmogorov-

TABLE 1. Experimental estimates of the model's parameters.

Parameter	Symbol	Value
Disease-induced decay (mortality) rate	α	1/15 d^{-1}
Transmission rate × Pathogen production rate*	$\nu\lambda$	0.00248 m²/d²
Disease decay rate	μ	0.002 d^{-1}
Initial population size	S_0	118.1 hosts/m
Diffusion coefficient	D	0.0274 m²/d

* Value is the average of the two replicates.

Smirnov test indicated that none of the four observed distributions of larvae differed significantly ($P < .05$) from that predicted from Eq. 15 using the value of D calculated from Eq. 16; in other words, there is no reason to reject diffusion as a model of the movement of tussock moth larvae. (The high coefficient of determination, r^2, of the regression is also encouraging but cannot be subjected to a significance test, as the sequential observations are of course not independent [Kareiva 1983].)

Testing the model

Table 1 lists the values of all the parameters in the model. Given these values, the model can be used in two complementary ways to predict a priori the rate of spread of the virus in the field. First, through numerical simulations I can use the model to predict the entire distribution of the infected fraction of the population. Second, using the wave speed calculation given in Appendix A, I can predict the rate of advance for the wave of infection. To tie these predictions to observations of the virus in the field, I performed an experiment in which I measured the rate of spatial spread of the virus. This task is of course very difficult, as I am attempting to predict quantitatively the dy-

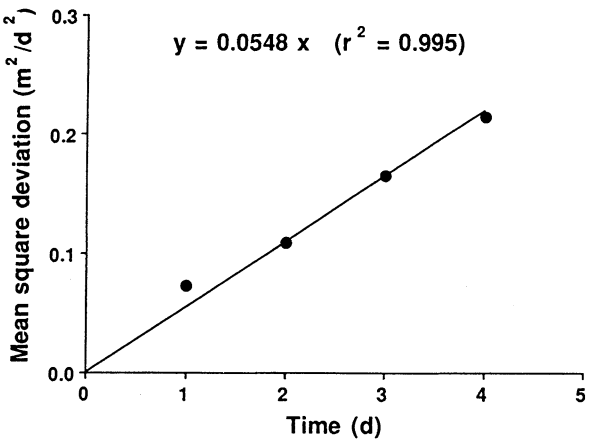

FIG. 8. Mean squared deviation of the position of tussock moth larvae dispersing from a point release on seedling Douglas-fir vs. the time since release.

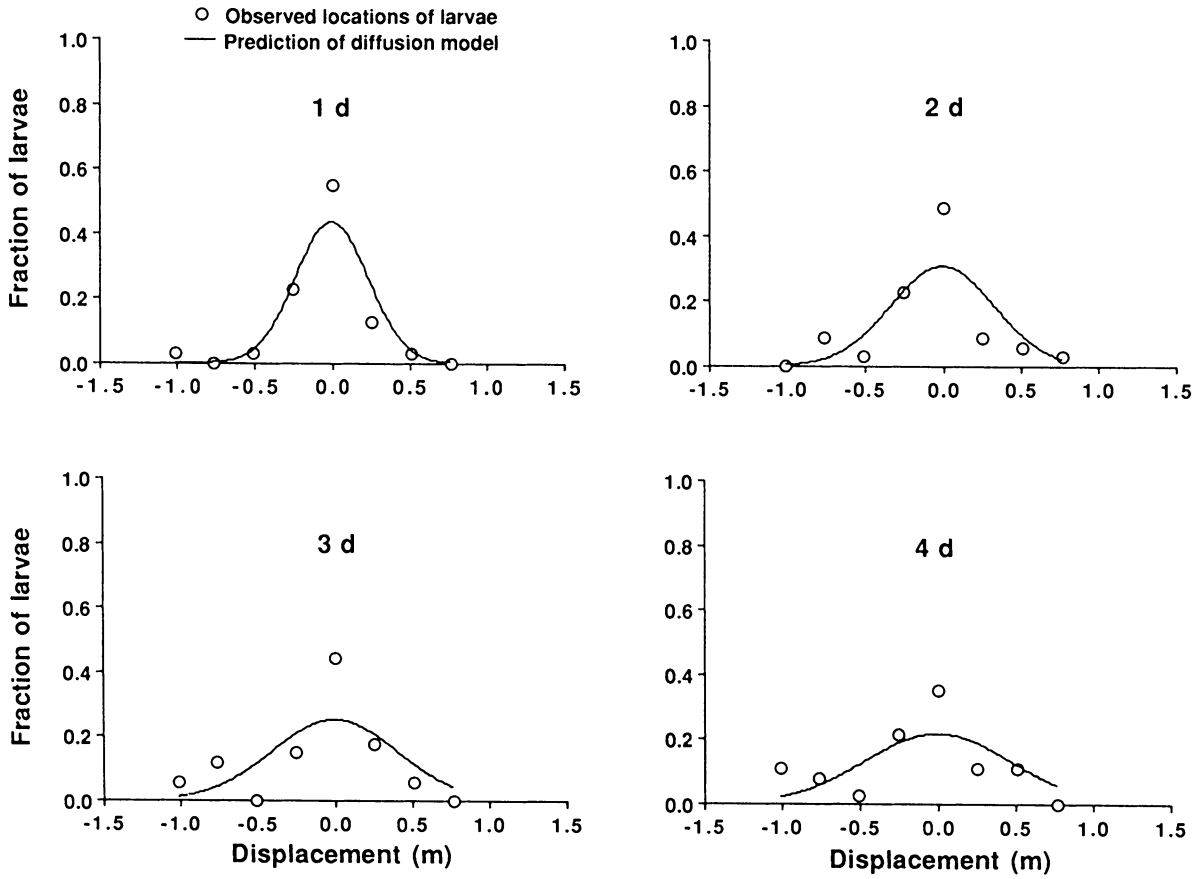

FIG. 9. Observed distribution of displacement of tussock moth larvae in the point release experiment 1, 2, 3, and 4 d after they were released, together with prediction of the diffusion model (Eq. 15), with the diffusion coefficient estimated from Fig. 8.

namics of an interspecific interaction from independent estimates of the parameters, so that even a qualitative fit between the model and the experimental data may be considered as support for the model (Kareiva and Odell 1987).

Methods.—To measure the spatial spread of the virus in the field, I released the virus into an experimental population of tussock moth larvae. The experimental setup was similar to that used to measure the movement rate of the insect; that is, I used eight seedling Douglas-fir set up ≈25 cm apart, in a line, with the trees again planted in sterile soil on plastic sheets surrounded by lawn edging coated with Tanglefoot. To prevent predation by vespid wasps, I set up tents of spun-bonded polyester (Reemay) around each array of trees. The tents were ≈1.5 m in height, and were supported by bamboo stakes.

To each tree in each linear array I added 30 healthy fifth-instar tussock moth larvae on 10 August 1990. To one of the end trees I added 20 larvae that had been infected with the virus 9 d earlier. These larvae were marked with fluorescent powder so that I could distinguish them from subsequent infections. All of the initially infected larvae were dead within 48 h. Because it is not always possible to tell whether dead larvae are infected without doing an autopsy, I had to remove all dead larvae to do autopsies. Removing larvae terminates the experiment, however, because the act of collecting dead larvae lowers the availability of virus. To measure the spatial spread of the virus I had to allow for multiple "cycles" of transmission, meaning that secondary infections could lead to tertiary infections, and so on, so that the amount of virus increased with time. My approach was therefore to initiate a wave of infection on six separate rows of trees and collect all the larvae from each of two rows of trees on three different dates. The treatments in this experiment thus consisted of three removal dates; that is, at 14, 28, and 35 d after the start of the experiment, I removed all living larvae from each of two rows and reared them in the laboratory until they pupated or died. Since each larva was reared separately on artificial diet, by removing the larvae to the laboratory I froze the virus spread at an instant in time. Although larval diet is known to affect disease susceptibility (Vail et al. 1968, Keating and Yendol 1987), what matters is what larvae

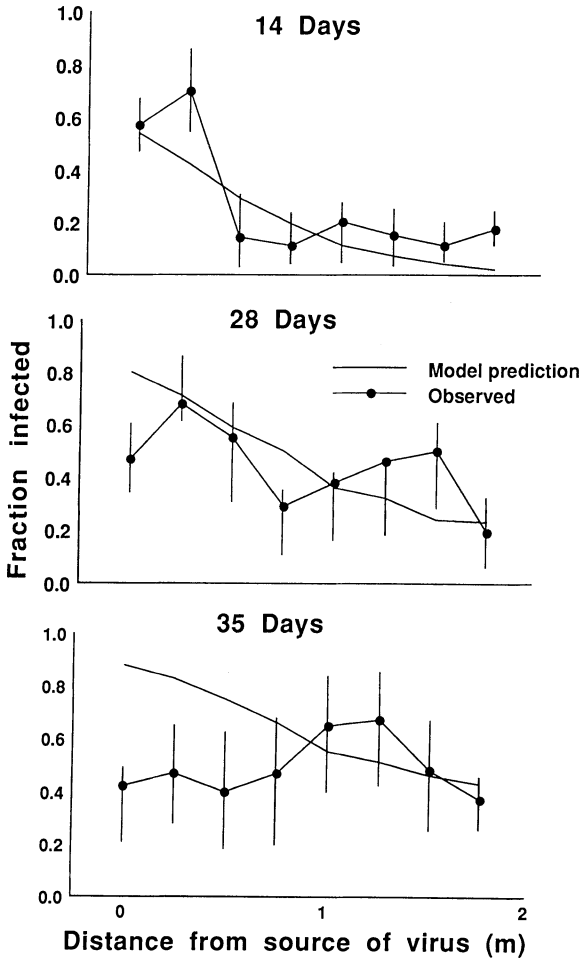

FIG. 10. Results of the nuclear polyhedrosis virus spatial spread experiment compared with predictions of the spatial model, using the parameter values in Table 1. Observed data points are for two replicates pooled. Vertical bars on observed data points indicate 95% binomial confidence intervals.

are eating when they are being exposed to the virus and not what they eat subsequently (M. Hunter, *personal communication*).

In sum, this experiment provided a snapshot of the spatial distribution of the infected fraction of the population at 14, 28, and 35 d after the release of the virus. What one expects to see qualitatively is that initially the infected fraction of the larvae will be high close to the source of the virus, but will fall off rapidly with distance. At later time intervals the fraction infected will still be high near the source of the virus, but will fall off less rapidly. This points out the ultimate necessity of the model; without it, it would be impossible to make an a priori prediction that is any more quantitative than this.

The three treatments were each replicated twice, and the rows of trees were arranged in two blocks of three rows each, with the blocks determined by amount of shade. In addition to the three experimental treatments, each block included a control row to which no infected larvae had been added, to act as a check for extraneous infections or accidental infections in the lab colony. Larvae in the control rows were not removed until the last removal date. No infections occurred in either control row. To test for infections that occurred in the laboratory, a corresponding group of control larvae was maintained in the laboratory for the duration of the experiment: no infections occurred in this group either.

Results.—The results of the experiment are plotted in Fig. 10. At 14 d a distinct wave is visible. At 28 d the shape of the wave is obscured by what is probably noise due to small sample size, although there still appears to be a rough gradient of disease incidence. At 35 d the sample sizes are so small that the estimates of the fraction infected are unreliable.

In Fig. 10 I also have plotted the prediction of the model for initial conditions corresponding to those of the field experiment; that is, a uniform distribution of 30 larvae per tree, and an initial density of 20 infected larvae on the first tree. Using the independently estimated parameters, the model predicts the shape of the wave at 14 d fairly accurately. The prediction is less accurate at 28 d, although the slope of the predicted curve is close to the average slope of the data. The model prediction for 35 d does not match the data at all.

Because the spatial domain of the experiment turned out to be small relative to the distance that the disease travels in 28 d, the shape of the travelling waves predicted by the model changes slightly with time. In other words, larvae reached the end of the row of trees quickly, so that the restraints imposed by the cage became important. Encouragingly, the model simulations accurately reflect this effect, in the sense that the theoretically predicted waves also did not maintain their exact shape with time: this can be seen more clearly in Fig. 1c. The analysis based on exact travelling waves does not take into account the spatial scale of the experiment, because it does not include any boundary effects. It is nevertheless interesting to compare the calculated and observed wave velocities in order to illustrate the method. Because at 35 d the sample sizes were very small and boundary effects predominated, I calculated the wave speed from only the first two time periods of the experiment. I estimated the wave speed from the data by calculating the velocity of different fractions of infected larvae. For a fraction infected of >0.10 and <0.55, the observed rate of advance of the disease is 0.09 m/d. For a fraction infected of 0.10, it is 0.15 m/d, and for a fraction infected of 0.55 it is 0.02 m/d. In spite of the distortion of the wave shape, this observed range of velocities compares reasonably well with the predicted value of 0.077 m/d.

Although small sample size undoubtedly is important, the poor match between model and data at 35 d could also be due to incorrect model formulation. One

of the advantages of using a reaction–diffusion model is that the epizootiology of the disease can be distinguished from the movement behavior of the host, making it easier to isolate errors in model construction. The epizootiology of the disease is undoubtedly oversimplified; among other things, transmission may not be linearly proportional to the densities of host and pathogen, and there is typically an incubation time between infection and death (Dwyer 1991). Field observations, however, suggested that a more significant error is that host movement behavior changes as foliage is consumed. By 35 d larvae had consumed most of the foliage on the experimental trees; a brief experiment confirmed that this leads to higher movement rates. I measured the diffusion coefficient D of fifth-instar larvae on defoliated and undefoliated trees by placing 40 larvae on a seedling Douglas-fir that was planted between two other seedlings in a line. In one treatment I used an undefoliated tree, while in the other I used a tree that had lost much of its foliage to larval feeding. The diffusion coefficient of larvae on the defoliated seedling, as measured over 2 h, was 0.0039 m^2/d, while the diffusion coefficient on the high-quality seedling was 0.0013 m^2/d. (The diffusion coefficient measured in this experiment is not comparable to that measured for the model because this experiment ran for <24 h, and tussock moth larvae have a distinct 24-h cycle of behavior [Edwards 1965].) This indicates that larvae do indeed have a higher movement rate on low-quality trees. In other words, although the model assumes a constant diffusion coefficient, in the experiment the diffusion coefficient increased as foliage quality declined. Although the larval densities that I used in the experimental test were in the range of densities observed in tussock moth outbreaks (Mason and Thompson 1971, Mason 1981), the small size of my experimental trees makes comparisons to natural densities difficult. As a result, it is not clear that natural outbreak densities would lead to sufficient defoliation to, in turn, increase larval movement enough to affect disease spread.

Discussion

Conventional factorial field experiments are designed to test specific hypotheses. The experimental test of the model that I present here is similarly designed to test a specific hypothesis, with the difference that here the hypothesis is represented by a mechanistic model. Given the small spatial and temporal scales of the experiment, however, my experimental setup was too crude to be considered more than a preliminary test of the model. Nevertheless, the model predictions were reasonably close to the data for the first 4 wk of the experiment. This at least *suggests* that the hypothesis embodied by the model is correct: host movement and host-pathogen interactions at a local scale are sufficient to predict the spatial spread of tussock moth NPV. Since all the model parameters were estimated independently, this is a stronger statement than saying simply that there was an effect of host movement, viral patchiness, and so forth.

Moreover, the parameters in the model were estimated at a scale that was about an order of magnitude smaller than the scale at which the model predicted the spread of the virus. Although the spatial scale of the experiment that I used to test the model was quite small, this feature of the model is common not just to reaction–diffusion models, but to so-called reaction–redistribution models, in which the assumption of diffusive movement is not required (Banks et al. 1987). This is significant because using information from small scales to predict large-scale dynamics is a central challenge in ecology.

Knowing the relationship between the characteristics of a pathogen, as represented by the model parameters, and the pathogen's rate of spatial spread, may have practical application in the release of genetically engineered insect viruses (J. P. Burand, *personal communication*). Before such viruses can be released in the field it is essential to know how far they will spread from the point of release. The wave speed calculation would be especially useful in this capacity because engineered viruses typically are designed to have a much shorter incubation time (larger α) and a much larger decay rate (larger μ) than wild-type viruses; given actual values of these parameters, the predicted wave speed could be obtained easily. In fact, since all of the model parameters can be estimated at a small scale, the model has the advantage that it does not require a field release to make predictions of the rate of spatial spread. That is, given laboratory estimates of the incubation time, transmission rate, and so forth, of the virus, it would be possible to predict the spatial rate of spread of an engineered virus, and thus the risk that such a virus would escape from a release site.

The experimental test of the model is necessarily specific to tussock moth and its NPV. It is important to emphasize, however, that no aspect of the model is specific to this particular insect host–pathogen system, and that the parameters could be estimated easily for other such diseases. As a result, the model should be applicable to other insect host–pathogen systems.

More generally, travelling wave models, such as Eqs. 7–9, should be useful in ecology as a whole, for several reasons. First of all, travelling waves are not specific to the model that I have presented, nor even to a small class of models, but can potentially occur in virtually any ecological model incorporating spatial structure (Keller and Segal 1971, Odell 1981, Okubo et al. 1989, van den Bosch et al. 1990). This *mathematical* ubiquity of travelling waves suggests that waves could result from a great many *biological* mechanisms. Indeed, travelling waves are apparent in disparate biological systems; examples include: (1) terrestrial plant succession (D. Doak, *personal communication*), (2) rocky intertidal patch dynamics (R. T. Paine, *personal com-*

munication), and (3) species invasions (Skellam 1951). Moreover, travelling wave models have important features that may not be apparent from the single application that I have presented here. The key characteristics of such models are (1) they are inherently non-equilibrium (Chesson and Case 1985); (2) they are capable of simultaneously predicting both spatial and temporal dynamics; (3) they can easily incorporate different interspecific interactions (Okubo et al. 1989); and (4) they are not limited to simple diffusion (Manasse and Kareiva 1990, van den Bosch et al. 1990). To date, travelling wave models have been largely the province of theoreticians (Skellam 1951, Levin 1981); their characteristics soon should make them more popular with empiricists.

ACKNOWLEDGMENTS

I would like to thank Garry Odell for hundreds of hours of help with the analysis and numerical simulation of the model. Trish Koehler and Chris Styles provided invaluable assistance in the field, in addition to being enormously entertaining and very supportive. The field site was provided at a very low cost by the University of Idaho, College of Forestry, Wildlife and Range Sciences, with the assistance and fence-building of Harold Osborne, manager of the Experimental Forest. Peter Kareiva, Joel Kingsolver, Bill Morris, Garry Odell, and Simon Levin made many helpful comments on the manuscript. I benefited greatly from the efforts of the editor Alan Hastings and two hard-working referees, Steve Vail and a second, anonymous, referee. Thanks also to Marilou Carlson, Gord'n Perrot, Trina Finholt, Joy Bergelson, and Viggo Andreasen for coming to visit. I was supported in part by a National Science Foundation Graduate Fellowship, and by National Science Foundation and USDA CSRS grants to Peter Kareiva.

LITERATURE CITED

Anderson, R. M., H. C. Jackson, R. M. May, and A. M. Smith. 1981. Population dynamics of fox rabies in Europe. Nature **289**:765–771.

Anderson, R. M., and R. M. May. 1981. The population dynamics of microparasites and their invertebrate hosts. Philosophical Transactions of the Royal Society, B, **291**: 451–524.

Banks, H. T., P. M. Kareiva, and K. A. Murphy. 1987. Parameter estimation techniques for interaction and redistribution models: a predator–prey example. Oecologia (Berlin) **74**:356–362.

Bird, F. T., and J. M. Burk. 1961. Artificially disseminated virus as a factor controlling the European spruce sawfly, *Diprion hercyniae* (Htg.) in the absence of introduced parasites. The Canadian Entomologist **93**:228–238.

Brookes, M. H., R. W. Stark, and R. W. Campbell, editors. 1978. The Douglas-fir tussock moth: a synthesis. United States Department of Agriculture Technical Bulletin **1585.**

Carruthers, R. I., and R. S. Soper. 1987. Fungal diseases. Pages 43–68 *in* J. R. Fuxa and Y. Tanada, editors. Epizootiology of insect diseases. John Wiley & Sons, New York, New York, USA.

Carter, J. B., E. I. Green, and A. J. Kirkham. 1983. A *Tipula paludosa* population with a high incidence of two pathogens. Journal of Invertebrate Pathology **42**:312–318.

Chesson, P. L., and T. J. Case. 1985. Overview: non-equilibrium community theories: chance, variability, history, and coexistence. Pages 229–239 *in* J. Diamond and T. J. Case, editors. Community ecology. Butterworth, New York, New York, USA.

Diekmann, O. 1979. Run for your life. A note on the asymptotic speed of propagation of an epidemic. Journal of Mathematical Biology **6**:109–130.

Dwyer, G. 1991. The effect of density, stage structure, and spatial structure on the transmission of an insect virus. Ecology **72**:559–574.

Dwyer, G., S. A. Levin, and L. Buttel. 1990. A simulation model of the evolution of myxomatosis. Ecological Monographs **60**:423–447.

Edwards, D. W. 1965. Activity rhythms of lepidopterous defoliators. III. The Douglas-fir tussock moth, *Orgyia pseudotsugata* (McDunnough) (Liparidae). Canadian Journal of Zoology **43**:673–681.

Entwistle, P. F., P. H. W. Adams, H. F. Evans, and C. F. Rivers. 1983. Epizootiology of a nuclear polyhedrosis virus (Baculoviridae) in European spruce sawfly (*Gilpinia hercyniae*): spread of disease from small epicentres in comparison with spread of baculovirus diseases in other hosts. Journal of Applied Ecology **20**:473–487.

Fleming, S. B., J. Kalmakoff, R. D. Archibald, and K. M. Stewart. 1986. Density-dependent virus mortality in populations of *Wiseana* (Lepidoptera: Hepialidae). Journal of Invertebrate Pathology **48**:193–198.

Fuxa, J. R. 1982. Prevalence of viral infections in populations of fall armyworm, *Spodoptera frugiperda,* in southeastern Louisiana. Environmental Entomology **11**:239–242.

———. 1987. Ecological considerations for the use of entomopathogens in IPM. Annual Review of Entomology **32**: 225–251.

Harkrider, J. R., and I. M. Hall. 1978. The dynamics of an entomopoxvirus in a field population of larval midges of the *Chironomus decorus* complex. Environmental Entomology **7**:858–862.

Hassell, M. P., and R. M. May. 1985. From individual behavior to population dynamics. Pages 3–32 *in* R. M. Sibly and R. H. Smith, editors. Behavioural ecology. Ecological consequences of adaptive behaviour. Blackwell, Oxford, England.

Hochberg, M. E. 1989. The potential role of pathogens in biological control. Nature **337**:262–264.

Kalmakoff, J., and A. M. Crawford. 1982. Enzootic virus control of *Wiseana* spp. in the pasture environment. Pages 435–438 *in* E. Kurstak, editor. Microbial and viral pesticides. Marcel Dekker, New York, New York, USA.

Kareiva, P. M. 1983. Local movement in herbivorous insects: applying a passive diffusion model to mark–recapture field experiments. Oecologia (Berlin) **57**:322–327.

Kareiva, P. M., and G. Odell. 1987. Swarms of predators exhibit 'preytaxis' if individual predators use area-restricted search. American Naturalist **130**:233–270.

Kaya, H. K., and J. F. Anderson. 1976. Biotic mortality factors in dark tussock moth populations in Connecticut. Environmental Entomology **5**:1141–1145.

Keating, S. T., and W. G. Yendol. 1987. Influence of selected host plants on gypsy moth (Lepidoptera: Lymantriidae) larval mortality caused by a baculovirus. Environmental Entomology **16**:459–462.

Keller, E. F., and L. A. Segal. 1971. Travelling bands of chemotactic bacteria: a theoretical analysis. Journal of Theoretical Biology **30**:235.

Kendall, D. G. 1965. Mathematical models of the spread of infection. Pages 213–225 *in* Mathematics and computer science in biology and medicine. Her Majesty's Stationery Office, London, England.

Klein, M., and H. Podoler. 1978. Studies on the application of a nuclear polyhedrosis virus to control populations of the Egyptian cottonworm, *Spodoptera littoralis.* Journal of Invertebrate Pathology **32**:244–348.

Levin, S. A. 1981. The role of theoretical ecology in the description and understanding of populations in heterogeneous environments. American Zoologist **21**:865–875.

Levin, S. A., and D. Pimentel. 1981. Selection for intermediate rates of increase in parasite–host systems. American Naturalist **117**:308–315.

Maddox, J. V. 1987. Protozoan diseases. Pages 43–68 *in* J. R. Fuxa and Y. Tanada, editors. Epizootiology of insect diseases. John Wiley & Sons, New York, New York, USA.

Manasse, R., and P. M. Kareiva. 1991. Quantitative approaches to questions about the spread of recombinant genes or recombinant organisms. Pages 215–231 *in* L. Ginzburg, editor. Assessing the ecological risk of biotechnology. Butterworth, New York, New York, USA.

Martignoni, M. E., and P. J. Iwai. 1980. Serum neutralization of nucleopolyhedrosis viruses (Baculovirus subgroup A) pathogenic for *Orgyia pseudotsugata*. Journal of Invertebrate Pathology **36**:12–20.

Mason, R. R. 1981. Numerical analysis of the causes of population collapse in a severe outbreak of the Douglas-fir tussock moth. Annals of the Entomological Society of America **74**:51–57.

Mason, R. R., and C. G. Thompson. 1971. Collapse of an outbreak population of the Douglas-fir tussock moth *Hemerocampa pseudotsugata* (Lepidoptera: Lymantriidae). United States Department of Agriculture Forest Service Research Note **PNW-139.**

May, R. M. 1974. Stability and complexity in model ecosystems. Second edition. Princeton University Press, Princeton, New Jersey, USA.

McLeod, P. J., S. Y. Young, and W. C. Yearian. 1982. Application of a baculovirus of *Pseudoplusia includens* to soybean: efficacy and seasonal persistence. Environmental Entomology **11**:412–416.

Mitchell, R. G. 1979. Dispersal of early instars of the Douglas-fir tussock moth. Annals of the Entomological Society of America **72**:291–297.

Mohamed, M. A., H. C. Coppel, and J. D. Podgwaite. 1983. Artificially induced nucleopolyhedrosis virus epizootic in populations of *Neodiprion sertifer* (Hymenoptera: Diprionidae). Environmental Entomology **12**:397–399.

Mollison, D. 1977. Spatial contact models for ecological and epidemic spread. Journal of the Royal Statistical Society, Series B, **39**:283–326.

Murdoch, W. W., J. Chesson, and P. L. Chesson. 1985. The theory and practice of biological control. American Naturalist **125**:344–366.

Murray, J. D. 1989. Mathematical biology. Springer-Verlag, New York, New York, USA.

Murray, J. D., E. A. Stanley, and D. L. Brown. 1986. On the spatial spread of rabies among foxes. Proceedings of the Royal Society of London, Series B, **229**:111–150.

Myers, J. H. 1981. Interactions between western tent caterpillars and wild rose: a test of some general plant herbivore hypotheses. Journal of Animal Ecology **50**:11–25.

Okubo, A. 1980. Diffusion and ecological problems: mathematical models. Springer-Verlag, New York, New York, USA.

Okubo, A., P. K. Maini, M. H. Williamson, and J. D. Murray, F.R.S. 1989. On the spatial spread of the grey squirrel in Britain. Proceedings of the Royal Society of London, Series B, **238**:113–125.

Odell, G. M. 1981. Appendix A.3: qualitative theory of systems of ordinary differential equations, including phase plane analysis and the use of the Hopf bifurcation theorem. Pages 590–623 *in* L. A. Segel, editor. Mathematical models in molecular and cellular biology. Cambridge University Press, London, England.

Olofsson, E. 1988. Environmental persistence of the nuclear polyhedrosis virus of the European pine sawfly in relation to epizootics in Swedish Scots pine forests. Journal of Invertebrate Pathology **52**:119–129.

Otvos, I. S., J. C. Cunningham, and R. I. Alfaro. 1987. Aerial application of nuclear polyhedrosis virus against Douglas-fir tussock moth, *Orgyia pseudotsugata* (McDunnough) (Lepidoptera: Lymantriidae). II. Impact 1 and 2 years after application. Canadian Entomologist **119**:707–715.

Podgwaite, J. D., P. Rush, D. Hall, and G. S. Walton. 1984. Efficacy of the *Neodiprion sertifer* (Hymenoptera: Diprionidae) nuclear polyhedrosis virus (Baculoviridae) product, Neochek-S. Journal of Economic Entomology **77**:525.

Podgwaite, J. D., K. S. Shields, R. T. Zerillo, and R. B. Bruen. 1979. Environmental persistence of the nucleopolyhedrosis virus of the gypsy moth, *Lymantria dispar*. Environmental Entomology **8**:528–536.

Robertson, J. 1985. *Orgyia pseudotsugata*. Pages 401–406 *in* P. Singh and R. F. Moore, editors. Handbook of insect rearing. Volume II. Elsevier, New York, New York, USA.

Seber, G. A. F. 1977. Linear regression analysis. John Wiley & Sons, New York, New York, USA.

Skellam, J. G. 1951. Random dispersal in theoretical populations. Biometrika **38**:196–218.

Shepherd, R. F., I. S. Otvos, R. J. Chorney, and J. C. Cunningham. 1984. Pest management of Douglas-fir tussock moth (Lepidoptera: Lymantriidae): prevention of an outbreak through early treatment with a nuclear polyhedrosis virus by ground and aerial applications. Canadian Entomologist **116**:1533–1542.

Stairs, G. R. 1965. Artificial initiation of virus epizootics in forest tent caterpillar populations. Canadian Entomologist **97**:1059–1062.

Thieme, H. R. 1977. A model for the spatial spread of an epidemic. Journal of Mathematical Biology **4**:377–351.

Thompson, C. G., and E. A. Steinhaus. 1950. Further tests using a polyhedral virus to control the alfalfa caterpillar. Hilgardia **19**:411.

Vail, P. V., T. J. Henneberry, A. N. Kishaba, and K. Y. Arakawa. 1968. Sodium hypochlorite and formalin as antiviral agents against nuclear polyhedrosis virus in larvae of the cabbage looper. Journal of Invertebrate Pathology **10**:84–93.

van den Bosch, F., H. D. Frinking, J. A. J. Metz, and J. C. Zadoks. 1988*a*. Focus expansion in plant disease. III. Two experimental examples. Phytopathology **78**:919–925.

van den Bosch, F., J. C. Zadoks, and J. A. J. Metz. 1988*b*. Focus expansion in plant disease. I. The constant rate of focus expansion. Phytopathology **78**:54–58.

van den Bosch, F., J. C. Zadoks, and J. A. J. Metz. 1988*c*. Focus expansion in plant disease. II. Realistic parameter-sparse models. Phytopathology **78**:59–64.

van den Bosch, F., J. A. J. Metz, and O. Diekmann. 1990. The velocity of spatial population expansion. Journal of Mathematical Biology **28**:529–566.

APPENDIX A

In this appendix I present the details of the calculation deriving the minimum possible rate of advance, or wave speed, of the disease for Eqs. 7–9. The calculations require no more than an understanding of the qualitative theory of ordinary differential equations (so-called "linear stability analysis"; see May [1974], Odell [1981], or Murray [1989]). I begin by non-dimensionalizing the model to reduce the number of parameters. If I let

$$s = \frac{\nu\lambda S}{\mu\alpha}, \tag{17}$$

$$i = \frac{\nu\lambda I}{\mu\alpha}, \tag{18}$$

$$p = \frac{\nu P}{\alpha}, \tag{19}$$

$$x = \left(\frac{\alpha}{D}\right)^{\frac{1}{2}} X, \tag{20}$$

$$t = \alpha T, \quad \text{and} \tag{21}$$

$$\rho = \frac{\mu}{\alpha}, \tag{22}$$

then Eqs. 7–9 become

$$\frac{\partial s}{\partial t} = -ps + \frac{\partial^2 s}{\partial x^2}, \tag{23}$$

$$\frac{\partial i}{\partial t} = ps - i + \frac{\partial^2 i}{\partial x^2}, \quad \text{and} \tag{24}$$

$$\frac{\partial p}{\partial t} = \rho(i - p). \tag{25}$$

(Note that the non-dimensionalization is such that non-dimensional space x is a linear function of dimensional space X. As a result, the wave speed is a linear function of the square root of the diffusion coefficient D.) If the solutions to the model form waves that travel with constant shape at a constant speed, then the model can be converted to a moving coordinate system using the transformation $\xi = x + ct$. This converts the system of partial differential equations to a system of ordinary differential equations, so that

$$cs' = -ps + s'', \tag{26}$$

$$ci' = ps - i + i'', \quad \text{and} \tag{27}$$

$$cp' = \rho(i - p), \tag{28}$$

where $'$ indicates differentiation with respect to ξ. To further convert this second-order system of three equations to a first-order system, I introduce the variables y and z such that $s' = z$ and $i' = y$, and obtain

$$s' = z, \tag{29}$$

$$z' = cz + ps, \tag{30}$$

$$i' = y, \tag{31}$$

$$y' = cy + i - ps, \quad \text{and} \tag{32}$$

$$p' = \frac{\rho}{c}(i - p). \tag{33}$$

This set of ordinary differential equations has two critical points (or equilibria). The first is at $(s,z,i,y,p) = (s_0,0,0,0,0)$, where s_0 is the initial value of s, which for convenience I take to be spatially uniform. This assumption is essential to the analysis, but is not necessary for the simulations. The second critical point is at the origin.

Numerical solutions indicate that travelling wave solutions only occur for $s_0 > 1$. Given that $s_0 > 1$, the numerical solutions show that the travelling waves proceed, in the phase space associated with Eqs. 29–33, from s_0 to another spatially uniform equilibrium $(s,z,i,y,p) = (s_\infty,0,0,0,0)$. I have not been able to generate an expression for s_∞, but the simulations indicate that s_∞ tends to decrease as s_0 increases; for s_0 much bigger than 1, s_∞ is close to zero.

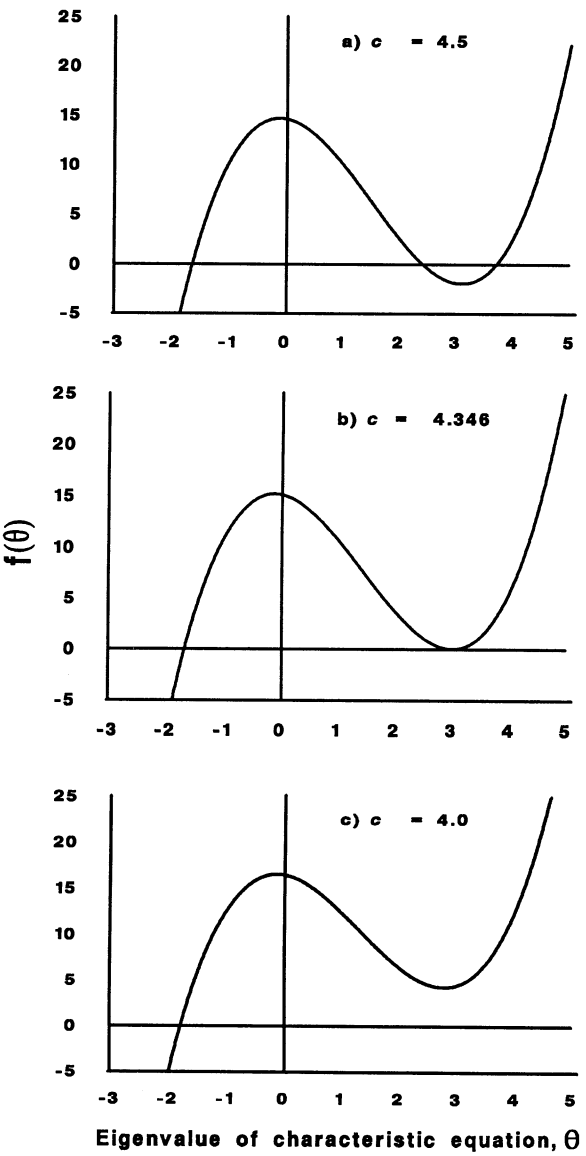

FIG. A1. Graph of Eq. 34 with parameters from Table 1. This demonstrates graphically the calculation of the minimum wavespeed c_{min}. As c is decreased, f looks successively like (a), (b), and (c). In (a), f has two real positive roots, in (c) f has two complex positive roots, and in (b) f has two (identical) real positive roots.

The calculation of the minimum possible wave speed proceeds from an analysis of the eigenvalues of the system of Eqs. 29–33 linearized around $(s_0,0,0,0,0)$. These eigenvalues are $\theta = 0$, c, and the roots of the cubic

$$f(\theta) = \theta^3 - \left(c - \frac{\rho}{c}\right)\theta^2 - (\rho + 1)\theta + \frac{\rho}{c}(s_0 - 1). \quad (34)$$

Since

1) $f(\pm \infty) = \pm \infty$,

2) $\left.\frac{\partial f}{\partial \theta}\right|_{\theta=0} < 0$, and

3) for $s_0 > 1$, $f(0) > 0$,

for any pair of values ρ and s_0, $f(\theta)$ looks like the curves in Fig. A1. As c is decreased, f will successively look like Figs. A1a, A1b, and A1c. If f looks like Fig. A1c, it will have one negative real root and a complex conjugate pair of roots, which means that near the critical point solutions will oscillate. Since at the critical point $i = p = 0$, so that oscillatory solutions imply negative population sizes, we can discard Fig. A1c. Fig. A1b thus represents the minimum possible value of c, denoted $c_{\min}$. For this minimum, $\frac{\partial f}{\partial \theta} = 0$ and $f = 0$, allowing us to eliminate θ to find $c_{\min}$ in terms of the other parameters. From this procedure, $c_{\min}$ is given by the positive root of $g(c^2_{\min})$, where

$$g(z) = 2z^3 + (3\rho + 9)z^2 - (27\rho s_0 + 3\rho^2 - 18\rho)z + 2[z^2 + z(\rho + 3) + \rho^2]^{3/2} - 2\rho^3. \quad (35)$$

For $s_0 > 1$, the information that

1) $g(0) < 0$,

2) $g(\pm \infty) = \pm \infty$, and

3) $\left.\frac{\partial g}{\partial z}\right|_{z=0} < 0$ for $s_0 > 1$,

can be used to sketch $g(z)$ to show that it has a unique positive root. This root is the minimum possible velocity for a travelling wave of disease, and can be calculated by a numerical root-finding routine. (The actual version of Eq. 35 used to generate Figs. 2, 3, 4, and 5 corresponds to the dimensionalized version of Eqs. 29–33.)

The sketches of $f(\theta)$ (Fig. A1) show that, for $s_0 > 1$, two eigenvalues have positive real parts, and one has a negative real part. Similar sketches of $f(\theta)$ for $s_0 < 1$ show that there will instead be one eigenvalue that has a positive real part, and two that have negative real parts. It is important to realize, however, that for Eqs. 29–33 the independent variable ξ is not the same as time t but is instead $x + ct$. The signs on the eigenvalues thus are not indicative of what one usually thinks of as stability (whether or not the populations will approach an equilibrium). This is because the direction of positive ξ is arbitrary, so that if Eqs. 29–33 are "unstable" for positive ξ, we can simply reverse the sign of ξ and they will be "stable." In short, the sign of the real part of the eigenvalues still indicates the direction of the flow around a critical point, but this is not the same as stability. Nevertheless, the fact that for $s_0 > 1$ there are two eigenvalues with positive real parts and one with a negative real part, while for $s_0 < 1$ there is one eigenvalue with a positive real part and two with negative real parts, indicates that it is at least topologically possible for a trajectory to proceed from an equilibrium at $(s_0 > 1,0,0)$ to $(s_0 < 1,0,0)$. (For $s_0 < 1$ it is again possible to use the argument that all eigenvalues must be real numbers to find a limit on the wave speed; the difference is that this analysis gives a maximum value for the wave speed.)

It remains to be shown that there is no trajectory from $[s_0 > (1,0,0,0,0)]$ to the origin. The eigenvalues of the system linearized about the origin are

$$\theta = 0, c, \frac{-\rho}{c}, \frac{c \pm \sqrt{c^2 + 4}}{2}. \quad (36)$$

In the vicinity of the origin, the trajectories that approach the origin will be governed by the solutions with negative eigenvalues, that is by

$$\theta = \frac{-\rho}{c}, \frac{c - \sqrt{c^2 + 4}}{2}. \quad (37)$$

The eigenvector associated with the eigenvalue $\frac{-\rho}{c}$ is the transpose of

$$[0, 0, 0, 0, A], \quad (38)$$

where A is a constant determined by the initial conditions. The eigenvector associated with $\theta = \frac{c - \sqrt{c^2 + 4}}{2}$ is the zero eigenvector. This means that trajectories that approach the origin do so in the $s = y = i = z = 0$ subspace (the p-axis). For the system Eqs. 29–33, again ξ is reversible, so that we can replace ξ by $-\xi$ and move backwards along any trajectory. If we make the substitution $\tau = -\xi$ in Eqs. 29–33 and move backwards from $s = y = i = z = 0$, we see that $s = y = i = z = 0$ for all positive τ regardless of the initial value of p. This means that any trajectory for which $s = y = i = z = 0$ had $s = y = i = z = 0$ for all previous ξ; in other words, any trajectory leaving $(s_0,0,0,0,0)$ will never reach the origin. In short, travelling wave solutions have trajectories that proceed from $(s_0 > 1,0,0,0,0)$ to $(s_0 < 1,0,0,0,0)$.

APPENDIX B

In this appendix I derive Eq. 14, which I use to estimate the parameter combination $\nu\lambda$ from the time series of infections in the 1-d treatment of the virus decay experiment. I begin by making two additional simplifications to Eqs. 4–6. First, since for the virus decay experiment all infected hosts were removed shortly after they died, there is no production of virus particles after the experiment begins. Second, as the virus decay experiment showed, there is no noticeable decay of virus over the course of a month. These two features of the experiment mean that the pathogen population P is constant, so that $P = P_0$, where P_0 is the initial input of the pathogen. The model that I use is thus

$$\frac{dS}{dT} = -\nu P_0 S; \tag{39}$$

$$\frac{dI}{dT} = \nu P_0 S - \alpha I; \quad \text{and} \tag{40}$$

$$\frac{dR}{dT} = \alpha I. \tag{41}$$

To match the data from the experiment, I have introduced the variable R, which is the cumulative number of infected hosts; the other symbols are the same as in Eqs. 4–6.

Eqs. 39–41 can be solved easily to give

$$R(t) = \frac{\alpha\nu P_0 S_0}{\nu P_0 - \alpha}\left[\frac{1}{\alpha}(1 - e^{-\alpha t}) - \frac{1}{\nu P_0}(1 - e^{-\nu P_0 t})\right]. \tag{42}$$

Next, I need the assumption that the number of pathogen particles per individual is constant, which is a reasonable assumption for my experiments, in which all larvae are fifth instars. This is equivalent to $P_0 = \Lambda I_0$, where Λ is the number of particles per individual, so that $\lambda = \Lambda\alpha$ (that is, the rate of production of particles is the number produced over the entire incubation period divided by the incubation period). Substituting $P_0 = \frac{\lambda}{\alpha} I_0$ into Eq. 42 gives

$$R(t) = \frac{\nu \frac{\lambda}{\alpha} I_0 S_0}{\nu \frac{\lambda}{\alpha} I_0 - \alpha}\left[\frac{1}{\alpha}(1 - e^{-\alpha t}) - \frac{\alpha}{\nu\lambda I_0}(1 - e^{-\nu \frac{\lambda}{\alpha} I_0 t})\right],$$

which is Eq. 14 in the main text.